chemosensors

MDPI

Article

Vibrational Analysis and Concentration Dependent SERS Study of Cefoperazone

Stefana Ana-Maria Faur [1], Zsejke-Réka Tóth [2], Klára Magyari [2] and Monica Baia [1,2,*]

[1] Faculty of Physics, Babes-Bolyai University, M. Kogalniceanu 1, 400084 Cluj-Napoca, Romania; stefana.faur@stud.ubbcluj.ro
[2] Nanostructured Materials and Bio-Nano-Interfaces Center, Interdisciplinary Research Institute on Bio-Nano-Sciences, Babes-Bolyai University, T. Laurian 42, 400271 Cluj-Napoca, Romania; zsejke.toth@ubbcluj.ro (Z.-R.T.); klara.magyari@ubbcluj.ro (K.M.)
* Correspondence: monica.baia@ubbcluj.ro

Abstract: Cefoperazone is a broad-spectrum antibiotic that is extremely efficient in the treatment of respiratory, abdominal, or genital infections. Vibrational spectroscopic techniques, FT-IR, Raman, and SERS, along with DFT calculations, were involved in investigating the normal modes of vibration and adsorption behavior of this antibiotic. Using both the experimental and theoretical data, the bands in the Raman and IR spectra were assigned to the normal vibrational modes. The SERS spectra were successively obtained by using silver and gold colloidal nanoparticles as a substrate. Their analysis revealed that the molecule is chemisorbed on the nanostructured surface through the as-denoted nitrogen ring. Changes observed in the SERS spectra recorded at different cefoperazone concentrations, i.e., modifications in the relative intensity of specific bands suggest the reorientation of adsorbed molecules towards the metal surface.

Keywords: cefoperazone; FT-IR spectroscopy; Raman spectroscopy; DFT calculations; SERS

Citation: Faur, S.A.-M.; Tóth, Z.-R.; Magyari, K.; Baia, M. Vibrational Analysis and Concentration Dependent SERS Study of Cefoperazone. *Chemosensors* **2024**, *12*, 48. https://doi.org/10.3390/chemosensors12030048

Received: 22 January 2024
Revised: 8 March 2024
Accepted: 16 March 2024
Published: 19 March 2024

1. Introduction

Medicine is increasingly emphasizing individualized diagnosis and treatment approaches for patients. While this path is still in its early stages, every incremental achievement made in this direction represents a significant stride toward realizing the ultimate goal of personalized healthcare. Cefoperazone, a third-generation cephalosporin antibiotic, has been a vital tool in combating bacterial infections for decades. With its broad spectrum of activity against a wide range of pathogens, cefoperazone has played a crucial role in clinical settings. However, there is still much to be discovered about this remarkable compound, particularly in terms of its molecular properties, interactions, and potential therapeutic applications. In recent years, there has been a growing interest in understanding the intricate workings of cefoperazone to unlock its full potential. It is used for the treatment of bacterial infections in various locations, including the respiratory tract, abdomen, skin, and female genital tracts [1–4], and is considered to be one of the few antibiotics effective against *Pseudomonas aeruginosa* [5]. Its action against streptococci (*S. aureus*, *S. penumoniae*, *S. pyogenes*), *Enterobacter* species, *Klebsiella pneumoniae*, or *E. coli* makes it a versatile drug to be used in severe infections in both adults and children. Clinical studies proved cefoperazone's efficiency in 92% of lower respiratory tract infections, 81% of urinary tract infections, 98% of gynecological infections, and 90% of a mixture of intra-abdominal, wound, and soft tissue infections. The clinical response was satisfactory in over 90% of infections with organisms normally susceptible to cephalosporins [6]. It acts by inhibiting the biosynthesis of cell wall mucopeptide, the third and last stage of bacterial cell wall synthesis. The chemical structure of cefoperazone plays an essential role in its functionality. Being a high protein-bound cephalosporin, it binds to specific penicillin-binding proteins located in the bacteria cell wall, through the β—lactam group [7]. Creating a thorough depiction of the

structural information of drugs and other substances is crucial, as it establishes a connection between their molecular structure and properties. To achieve this, employing vibrational spectroscopic methods in conjunction with density functional theory (DFT) calculations proves to be a precise approach [8–16].

Gold and silver nanoparticles have been extensively studied in the past decade, for their great interest in the field of nanomedicine. They display a great potential for diagnosis and personalized treatment either as a substrate for SERS investigations [17–19] or by themselves, considering the fact that they can improve antimicrobial activity [20]. A lot of antibiotics such as levofloxacin, tetracycline, benzylpenicillin [11], sulfathiazole [21,22], quinolones [23], ciprofloxacin [24], and many others [17] have been studied through the SERS method. It has also been shown that antibiotic-functionalized gold nanoparticles can detect β-lactamase and be used as a useful tool in combating antimicrobial resistance [25].

The existing literature mentions few studies dedicated to the vibrational analysis of cephalosporins, focusing rather on FT-IR spectroscopy [26–28]. However, recent works concentrate on SERS investigations of cephalosporins (including cefoperazone) for their detection in urine, using either copper [29] or silver [30] nanoparticles. Also, the molecular electrostatic potential of the cefoperazone molecule was obtained by DFT calculations, using the BP86-D3 functional and the 6-31G (d, p) basis set [31]. The aim of this study is to provide additional information on the vibrational analysis of cefoperazone and its adsorption behavior at different analyte concentrations by analyzing SERS spectra obtained using colloidal gold and silver nanoparticles. This comprehensive vibrational analysis of cefoperazone will provide new insights that could open ways for further applications.

2. Materials and Methods

2.1. Materials

The cefoperazone sodium salt used in this study was purchased from Alfa Aesar, by Thermofisher Scientific, Waltham, MA, USA. It comes as white to pale cream crystalline powder, soluble in water and slightly soluble in alcohol. All other compounds involved in colloids and solutions preparation were purchased from Sigma Aldrich as analytical pure reagents.

2.2. Synthesis of Ag Nanoparticles

The synthesis of silver colloidal nanoparticles (AgNPs) was completed following the method proposed by Lee and Meisel [32], by reducing the silver nitrate ($AgNO_3$) with trisodium citrate dihydrate ($C_6H_5O_7Na_3 \cdot 2H_2O$). An $AgNO_3$ aqueous solution was prepared, by adding 90 mg of $AgNO_3$ to 500 mL water. Then, it was brought to boiling. Over the boiling $AgNO_3$ solution, 10 mL of trisodium citrate dihydrate was added. The final solution was maintained boiling for approximately an hour. As one can see from Figure S1a (Supplementary Materials) the obtained grey–yellow solution presents a broad absorption peak with a maximum at 432 nm due to the localized surface plasmon resonance (LSPR) of AgNPs with a mean particle size of around ~60 nm in diameter.

2.3. Synthesis of Au Nanoparticles

Gold nanoparticles (AuNPs) were prepared according to the Turkevich method [33], by reduction of hydrogen tetrachloroaurate (III) with trisodium citrate dihydrate. Thus, 21.2 mg of chloroauric acid ($HAuCl_4 \cdot 3H_2O$) was dissolved in 25 mL ultrapure water, then heated to the boiling point. A 750 µL amount of 1% citrate solution was added to the boiling solution while kept boiling under magnetic stirring for 20 min. After about a minute, a very faint greyish-pink or greyish-blue tone must appear and in a period of five minutes, it darkens to deep wine and red color. The synthesized nanoparticles were almost spherical, and their estimated mean diameter was 62 nm as derived based on the λ_{max} of the LSPR absorption observed at 537 nm. The UV–VIS absorption spectrum of the colloid is illustrated in Figure S1b (Supplementary Materials).

2.4. Fourier Transform Infrared Spectroscopy Measurements

The FT-IR absorption spectrum of the cefoperazone sample was recorded with 256 scans and one acquisition with a JASCO FT-IR 6600 spectrometer, at room temperature, in the 400–4000 cm^{-1} range with a spectral resolution of 4 cm^{-1}, by using the KBr pellet method. Corrections of the spectrum were made, by subtracting the KBr, water, and CO_2 contributions.

2.5. Raman Spectroscopy and SERS Measurements

For the acquisition of the Raman and SERS spectra, a confocal Renishaw InVia Reflex Raman spectrometer was used. The Raman spectra of cefoperazone were recorded, using a 100× (NA 0.75) microscope objective and a grating of 1800 lines/mm. The Raman spectra of bulk material were recorded using two laser lines: 532 nm (Cobalt, Diode Pumped Solid State), power 200 mW, but used only at 10%, with an acquisition time of 3 s, and 633 nm (gas, He-Ne), power 17 mW, with an acquisition time of 20 s. The Raman spectra of the Ag and Au colloidal suspensions were also recorded, and no bands were observed (see Figure S2, Supplementary Materials).

SERS spectra were recorded from different sites of the flat substrates created by drying out the solutions of cefoperazone and silver or gold colloids. A 10 mL amount of aqueous solution of 10^{-2} M cefoperazone was prepared, along with the dilutions of 10^{-3} M to 10^{-6} M. Dilutions of 10^{-2} M cefoperazone solution were subsequently made by using ultrapure water in order to obtain different concentrations. For each concentration, 25 µL of antibiotic solution was combined with 25 µL of silver colloid and 25 µL of gold colloid, respectively. A droplet of each solution was deposited on a glass slide covered by parafilm and let overnight, for water to evaporate.

SERS spectra were also acquired with the 100× (NA 0.75) microscope objective and a grating of 1800 lines/mm. Because of the different plasmonic responses of AgNPs and AuNPs, different laser lines were used to record the spectra of cefoperazone adsorbed on silver colloid and gold colloid, respectively. For the first one, we used the 532 nm laser line, while for the latter we chose the red laser, at 633 nm. Multiple spectra were recorded for each concentration, by varying the parameters of acquisition (time, laser power), in order to find the best results and the least noise. The optimal parameters found for each acquisition are reported in Table 1.

Table 1. Optimal parameters for the SERS spectra acquisition.

	Concentration (M)	Acquisition Time (s)	Laser Power (mW)
Cefoperazone + colloidal AgNPs 532 nm	10^{-2}	5	2
	10^{-3}	3	2
	10^{-4}	3	2
	10^{-5}	5	2
	10^{-6}	5	2
Cefoperazone + colloidal AuNPs 633 nm	10^{-2}	15	0.17
	10^{-3}	15	0.17
	10^{-4}	5	0.17
	10^{-5}	15	0.17
	10^{-6}	10	0.17

2.6. Computational Details

The optimized geometry of the cefoperazone molecule, together with the theoretical IR and Raman spectra, were obtained using DFT methods. The calculations performed with the Gaussian 09 software [34] used two functionals: Becke's 1988 exchange functional and the Perdew–Wang 91 gradient-corrected correlation functional (BPW91) [35] and Becke's three-parameter hybrid method using the Lee–Yang–Parr correlation functional (B3LYP) [36]. 6-311+G(d) was used as the basis set. The assignment of the theoretical wavenumber values to the corresponding vibrational modes was performed by visually observing the normal modes in the GaussView program.

3. Results and Discussion

3.1. Vibrational Analysis

The cefoperazone molecule is composed of 71 atoms, arranged in various functional groups. The optimized geometry obtained through DFT calculations with the labeling of the atoms is depicted in Figure 1.

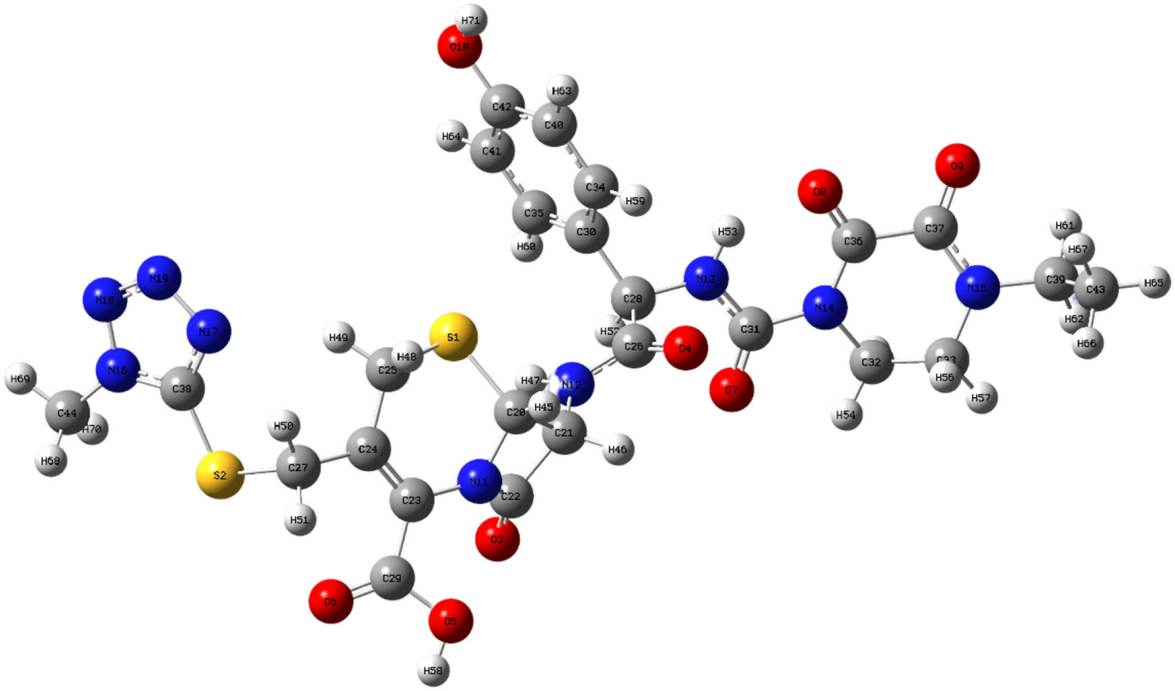

Figure 1. The optimized geometry of the cefoperazone molecule.

Because of the relatively large number of atoms, the symmetry of cefoperazone is low. However, the functional groups within this molecule are numerous and some may present local symmetry, such as the benzene ring or the hexagonal heterocycle. Among these functional groups (see Figure 2), one can distinguish the benzene ring, the ring containing four nitrogen atoms ($C_{38}N_{17}N_{19}N_{18}N_{16}$), specific to cefoperazone that will hereafter be called the nitrogen ring, then the β–lactam group and the carboxylate group (both specific to penicillins and cephalosporins). These groups have the potential to play an important role in the SERS analysis, contributing to the molecule adsorption to the nanostructured metallic surface. As one can see from Figure 1, due to the geometry of the molecule, the nitrogen and benzene rings might be more likely to interact with the surface of colloidal nanoparticles compared to other parts of the molecule.

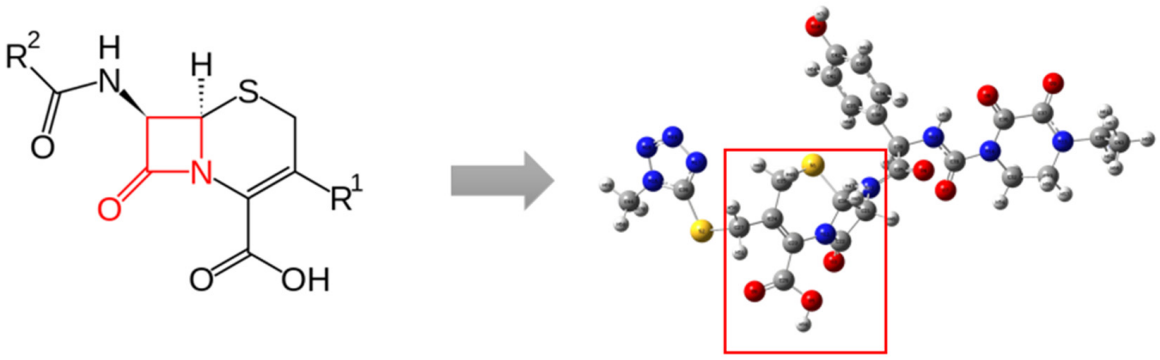

Figure 2. Functional group specific to cephalosporins. β–lactam is marked in red.

The theoretical calculations successfully predicted the vibrational modes and demonstrated excellent agreement with the experimental results. No imaginary frequency modes were obtained at all theoretical levels, indicating that the structures are at a local minimum on the potential energy surface. Furthermore, the number of vibrational modes obtained, which was 207, aligns perfectly with the theoretical formula for the number of vibrational modes in nonlinear molecules, namely 3N-6 (where N represents the atom number). Based on these findings, we can confidently conclude that the structures analyzed are in a stable state on the potential energy surface. To comprehend and anticipate the interaction between cefoperazone and plasmonic structures, the molecular electrostatic potential (MEP) was computed for the optimized geometry of the theoretical model. The outcomes of the B3LYP/6-31+G(d) calculations are depicted in Figure 3 as a 3D RGB map of the optimized cefoperazone. Based on the information illustrated in Figure 3, and having in mind that an increased negative charge on an atom increases the atom's probability to act as an adsorptive site [37], it becomes obvious that the regions with elevated electron density, specified by red and yellow colors, indicate potential sites for cefoperazone adsorption on the colloidal nanoparticles surface. However, the adsorption of the molecule on the substrate is fully elucidated based on the analysis of the SERS spectra.

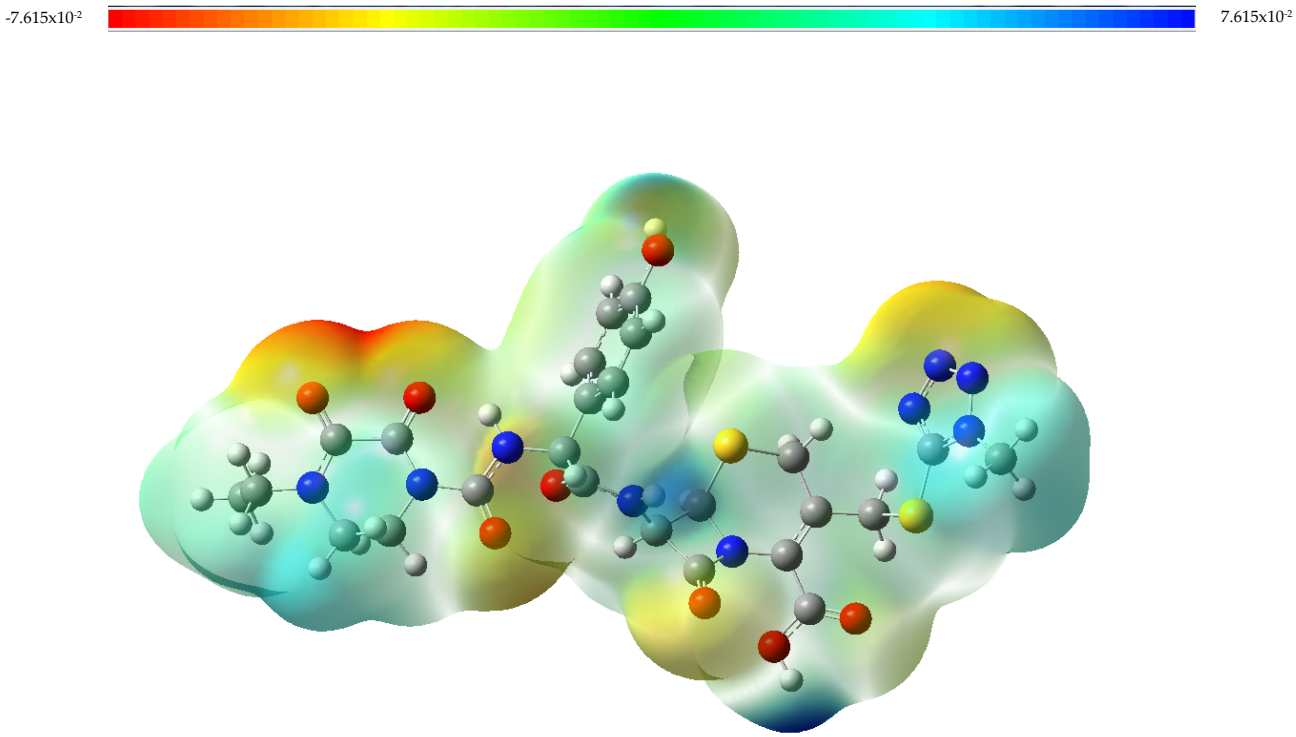

Figure 3. Molecular electrostatic potential of cefoperazone generated at the B3LYP/6-31+G(d) theoretical level.

The Raman and FT-IR spectra of cefoperazone are illustrated in Figure 4. For each technique, we chose to display the spectra in a comparative manner, by overlaying the experimental results and the simulations generated at both theoretical levels. At first glance, the experimental and theoretical spectra present a great resemblance, for both Raman and IR. They keep the same allure. Nonetheless, as expected, there are some differences between them. The discrepancy between the experimental wavenumber values and the calculated ones might be a consequence of anharmonicity but also might be because of the computational methods and different approximations.

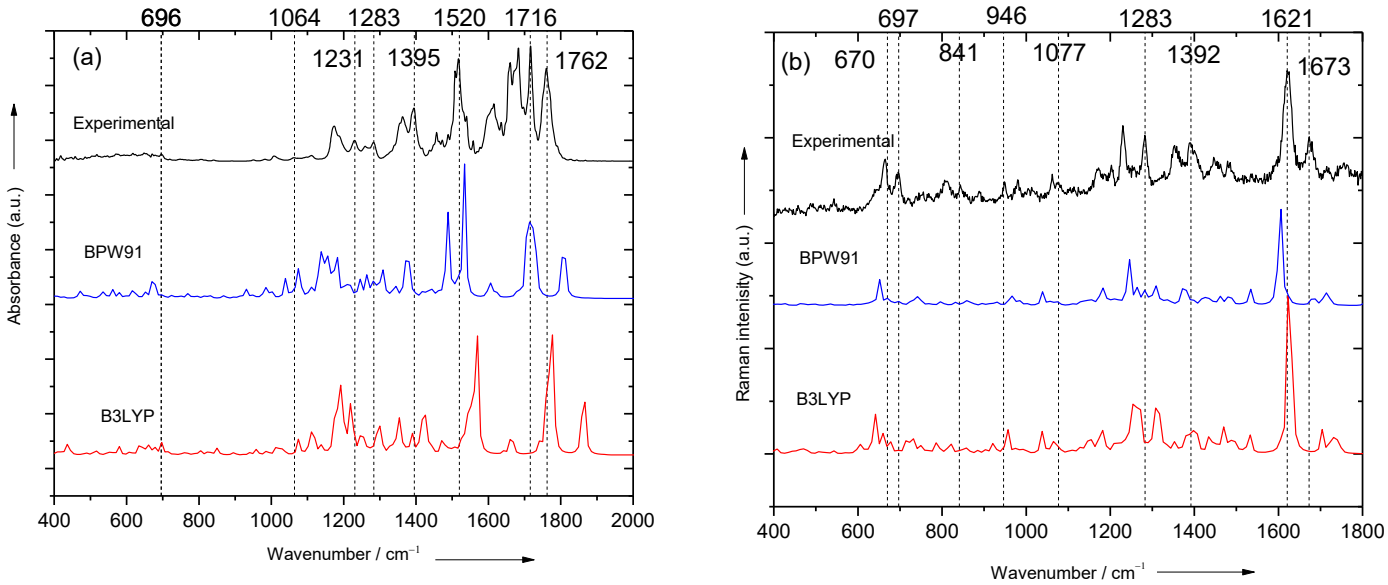

Figure 4. Experimental and theoretical (BPW91 and B3LYP) FT-IR (**a**) and Raman (**b**) spectra of cefoperazone. The FWHM of the theoretical spectra is 4 cm^{-1}.

The wavenumber values of vibrational modes obtained using the BPW91 functional were closer to those of the bands in the experimental spectra. BP3LYP tended to overestimate these values. However, in some wavenumber regions, B3LYP displayed a better approximation than BPW91. These regions are around 600–700 cm^{-1} and 1600–1800 cm^{-1}. By looking at Figure 4, it becomes evident that the bands in the spectra generated using the B3LYP functional exhibit a closer overlap with the experimental data in those particular regions. In contrast, the bands associated with the BPW91 functional display a blue shift, indicating a shift towards higher frequencies compared to the experimental bands.

The vibrational modes assignment was completed by visually observing the normal modes in the GaussView program and were further compared to the existing literature dedicated to the vibrational analysis of cephalosporins [26–28]. Thus, the experimental and theoretical results were corroborated and are summarized in Table 2.

At lower wavenumbers, vibrations of the whole molecule occur. They are very low in intensity and consist of slight changes in the dihedral angles between the planes of the bonds. At 212 cm^{-1}, the out-of-plane deformation of the nitrogen ring can be seen.

Regarding the benzene ring, the hydrogen atoms (H_{64}, H_{63}, H_{59}, H_{60}) execute all types of deformation, with respect to the ring and to one another: wagging at 810 cm^{-1}, rocking at 851 cm^{-1}, twisting at 1170 cm^{-1}, scissoring at 1447 cm^{-1}. The "breathing" vibration of the ring is reported by the DFT calculations to be around 835 cm^{-1}, but the corresponding band in the experimental Raman spectrum can be found at 841 cm^{-1}.

In addition to the bands due to the aromatic ring vibrations, the most numerous bands in the spectra correspond to the nitrogen ring ($C_{38}N_{17}N_{19}$ $N_{18}N_{16}$) vibrations. Consisting of two double bonds (N=N and C=N) and two simple bonds (C-N and N-N), this ring displays various modes of vibration. The out-of-plane deformation of the whole ring can be found at 212 cm^{-1}. At 664 cm^{-1}, a double-twisting within this ring can be found between the C_{38}=N_{17}-N_{19}=N_{18} atoms. This means that the C_{38} and N_{19} move in phase, as well as N_{17} and N_{18}, resulting in a double-twisting centered around the N_{17} and N_{19} atoms. A similar vibration occurs at 697 cm^{-1}. This time, the twisting is centered around the N_{16} and N_{18} atoms. Around 1070 cm^{-1}, an asymmetric stretching vibration takes place, belonging to the N_{16}-N_{19}=N_{18} bonds. There is a very intense band in the Raman spectrum at 1280 cm^{-1}, corresponding to the N_{19}=N_{18} stretching vibration.

Table 2. Assignment of the vibrational modes of cefoperazone.

Experimental		Theoretical		Assignment
IR	**Raman**	**B3LYP**	**BPW91**	
	212	207	200	Out-of-plane deformation of $C_{38}N_{17}N_{19}N_{18}N_{16}$ ring
457		445	428	In-plane deformation of $C_{38}N_{17}N_{19}$ $N_{18}N_{16}$ ring
	664	677	647	$N_{18}N_{19}C_{38}$ twist + $N_{16}N_{18}N_{19}$ twist
670	675	677	652	$C_{27}S_2$ stretch
696	697	791	691	$N_{19}N_{17}C_{38}$ twist + $N_{17}N_{19}N_{18}$ twist
	810	833	818	Wagging of H atoms from the aromatic ring
	841	856	833	$C_{40}C_{42}C_{40}$ + $C_{34}C_{30}C_{35}$ bending (breathing-like vibration of aromatic ring)
	851	882	855	$H_{50}C_{27}H_{51}$ rock + $H_{48}C_{25}H_{49}$ rock
	946	988	946	$N_{18}N_{16}$ str + $C_{38}N_{17}N_{19}$ sym str
1008	1013	1032	1002	$C_{40}C_{42}C_{40}$ + $C_{34}C_{30}C_{35}$ bending + $C_{40}H$+$C_{41}H$ bending
1064	1077	1063	1073	$N_{17}N_{19}N_{18}$ asym str
1109	1170 1188	1191	1108	Twisting of H atoms from the aromatic ring
1231	1230	1274	1232	$C_{33}N_{15}$ str + $C_{32}N_{14}$ str
1283	1283	1345	1280	$N_{18}N_{19}$ str
1362	1355	1390	1342	$H_{61}C_{39}H_{62}$ wag + $H_{57}C_{33}H_56$ wag + $H_{54}C_{32}H_{55}$ twist
	1388	1421	1379	$C_{23}N_{11}$ str + $C_{38}N_{17}$ str + $O_5C_{29}H_{58}$ scissoring
1395	1392		1395	$C_{38}N_{16}$ str
	1403	1471	1419	$C_{37}N_{15}$ str + $H_{56}C_{32}H_{57}$ wag
	1447	1474	1435	$H_{50}C_{27}H_{51}$ scissoring + $H_{48}C_{25}H_{49}$ scissoring
1456	1486	1480	1440	Scissoring of H atoms of the benzene ring
		1485–1568	1446–1489	Deformations of CN bonds
1520		1547		$C_{26}N_{12}$ str
1540		1568	1533	$C_{31}N_{13}$ str
		1641	1595	Asymmetric stretching of the aromatic ring
1597		1663	1603	C_{23}=C_{24} str
1615	1621	1665	1619	Symmetric stretching of the aromatic ring
1683	1673	1726	1682	$C_{36}O_8$ stretch
		-	1706	$C_{37}O_9$ str
1716	1712	1766	1712	$C_{26}O_4$ str
			1719	$C_{29}O_6$ str
			1727	$C_{31}O_7$ str
1762	1754	1863	1808	$C_{22}O_3$ str
		3024–3215	2960–3150	C-H str
3317		3500	3336	$N_{13}H_{53}$ str
3560		3605	3502	$N_{12}H_{47}$ str
3588		3693	3582	O_5H_{58} str
3735		3750	3638	$O_{10}H_{71}$ str

str = stretching, wag= wagging, twist = twisting, rock = rocking, sym = symmetrical, asym = asymmetrical.

The vicinity of the atoms plays a crucial role in vibrational spectroscopy. We have noticed that the atoms with similar neighboring give normal modes at the same frequency. For instance, at 851 cm^{-1}, one can find the rocking motions of the $H_{50}C_{27}H_{51}$ and $H_{49}C_{25}H_{48}$ groups. Both carbons are neighboring the sulfur atoms. The scissoring vibration of the same groups is found again at the same wavenumber, that is 1447 cm^{-1}. The same phenomenon happens around 1350 cm^{-1} in both Raman and IR spectra. At this wavenumber value, vibrations involving the carbons neighboring the nitrogen atoms occur, namely the wagging of $H_{61}C_{39}H_{62}$ and $H_{57}C_{33}H_{56}$ and the twisting of $H_{55}C_{32}H_{54}$ groups.

Between 1600 and 1800 cm^{-1}, more IR active vibrations can be found. Here, the stretching modes of C=O bonds can be found. These represent the most intense bands in the IR spectrum of cefoperazone. Some of them can also be seen in the Raman spectrum but with a much lower intensity. Those would be at 1712 cm^{-1} and 1754 cm^{-1}, assigned to the C_{36}=O_8 and C_{37}=O_9 bonds, respectively. Again, this is in good agreement with the selection rules, as they are situated in a region with local symmetry.

In the range of high wavenumber values (see Figure S3, Supplementary Materials), starting with 2900 cm^{-1}, lie the stretching vibrations of simple bonds. In the 2900–3150 cm^{-1} range, one can find the stretchings of H-C-H bonds. Above the value of 3150 cm^{-1}, the stretching vibrations of N-H and O-H bonds occur, for various pairs of atoms.

3.2. Adsorption of Cefoperazone on Gold and Silver Colloidal Nanoparticle Surfaces

The adsorption behavior of the cefoperazone molecule was assessed through the analysis of two sets of SERS spectra recorded by using gold and silver colloidal nanoparticles as SERS substrates. Comparison of SERS and Raman spectra (see Figures 5 and 6) reveals shifts and changes in the relative intensities of the bands in the SERS spectra in comparison to the corresponding ones in the normal Raman spectrum. Moreover, it is important to note that the intensities in the Raman spectrum for each set were multiplied to ensure visibility when compared to the SERS spectra. This enhancement can be observed through the presence of noise in the spectra.

The SERS spectra are directly dependent on the concentration of the antibiotic in an aqueous solution. Changes associated with the concentration modifications are due to a reorientation of the adsorbed molecules with respect to the metallic surface or to different interactions between the analyte and the nanostructured surface [38–41]. A selection of the enhanced Raman bands with the corresponding vibrations is summarized in Table 3.

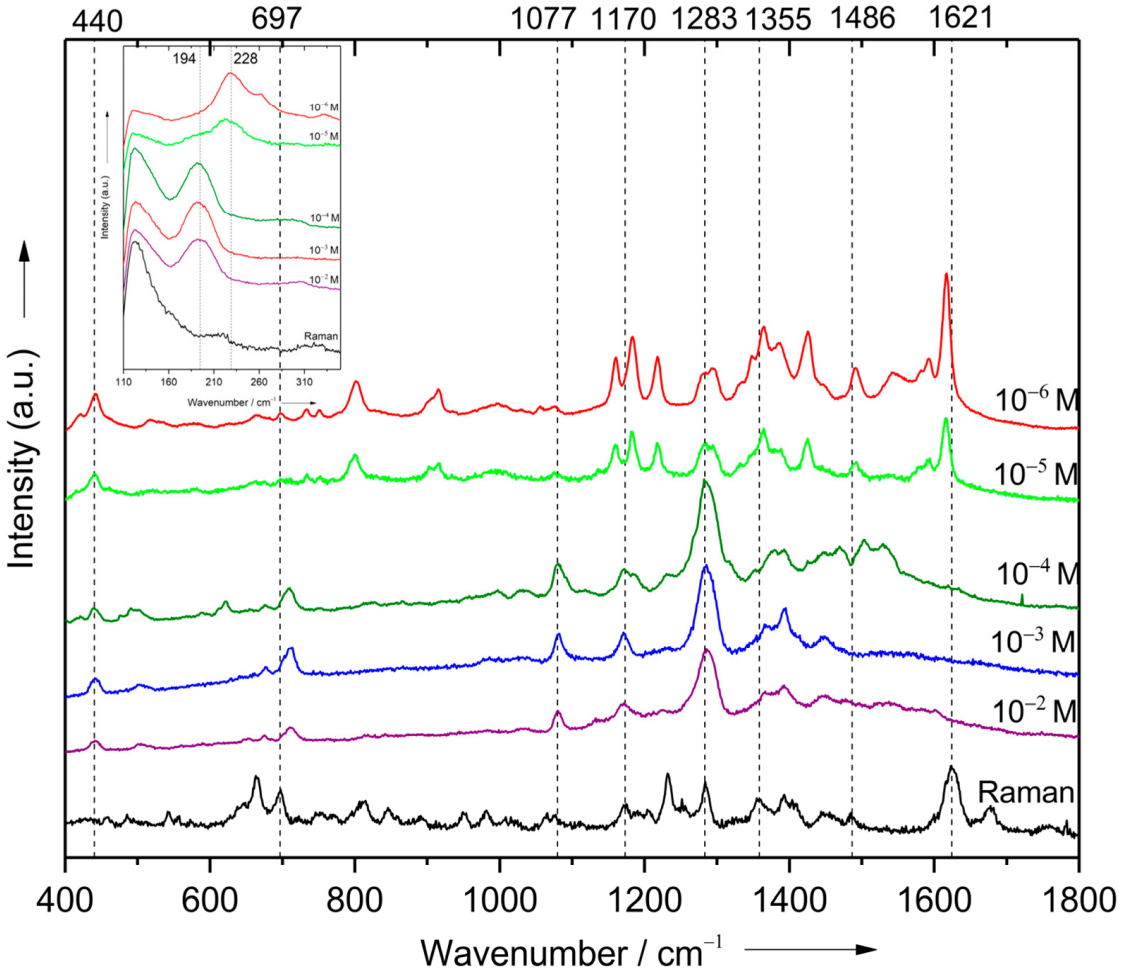

Figure 5. SERS spectra of cefoperazone adsorbed on gold nanoparticle surface at different concentrations, as indicated. For comparison, the Raman spectrum is also illustrated and multiplied 10 times to ensure visibility.

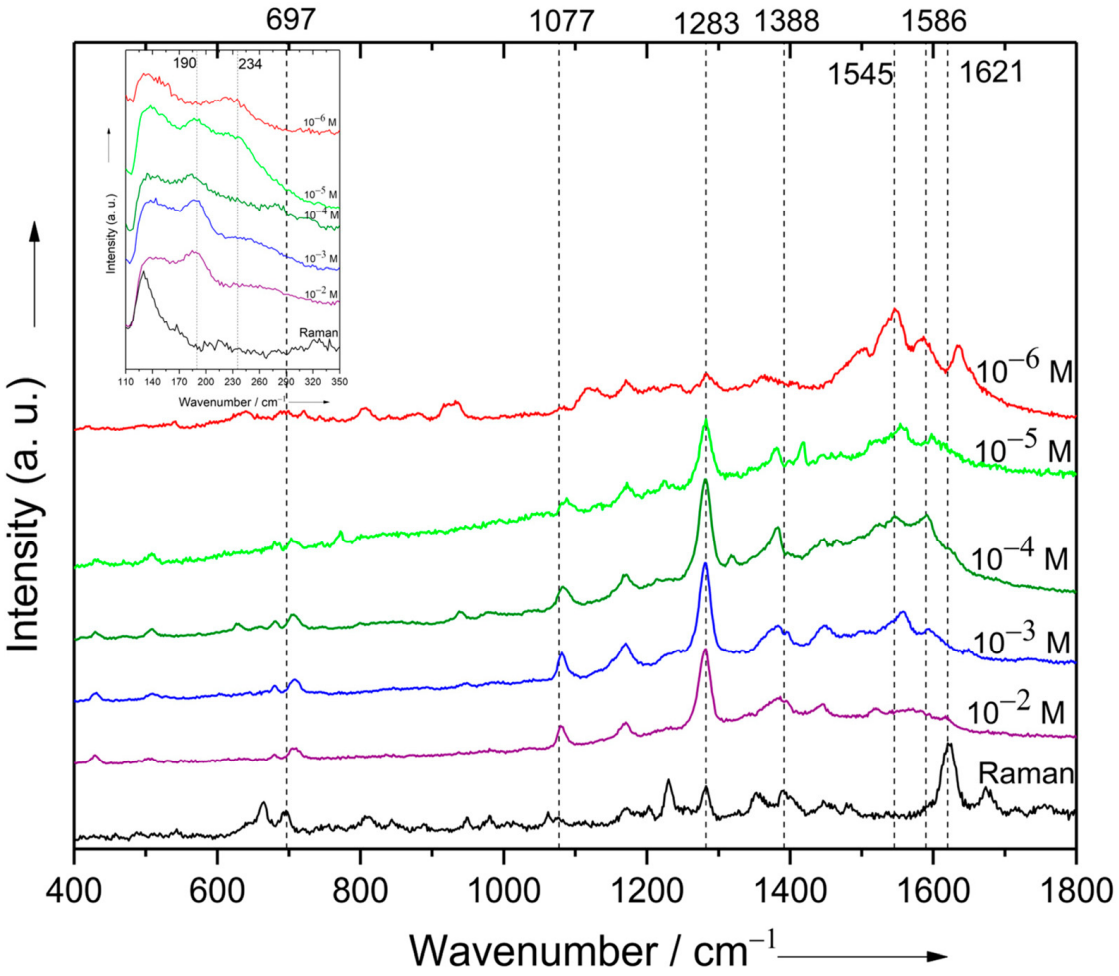

Figure 6. SERS spectra of cefoperazone adsorbed on silver nanoparticles surface at different concentrations, as indicated. For comparison, the Raman spectrum is also illustrated and multiplied 10 times to ensure visibility.

The similarity between the spectra of cefoperazone adsorbed on the surface of AuNPs from concentrations of 10^{-2} M to 10^{-4} M is striking, as can be seen in Figure 5. The same vibrations are enhanced in all three spectra. Furthermore, a similar spectral pattern was evidenced in the SERS spectra recorded by Markina et al. [30]. The most enhanced band is that at 1283 cm^{-1} due to the stretching vibration of the $N_{18}N_{19}$ bond. Moreover, one can notice the band at 1080 cm^{-1} assigned to the asymmetric stretching vibration of the $N_{17}N_{19}N_{18}$ group. The band at 697 cm^{-1} in the Raman spectrum is enhanced and shifted to 706 cm^{-1} in the SERS spectra at concentrations higher than 10^{-4} M. It corresponds to the double-twisting of the C_{38}=N_{17}-N_{19} and N_{17}-N_{19}=N_{18} bonds.

These shifts show there was a change in the energy levels of the molecule. According to the charge transfer theory [33], when the molecules are chemisorbed on the metallic surface, a new bond is formed between the metal nanoparticle and the adsorbed molecule that will lead to the appearance of a new band in the SERS spectrum and also to shifts or changes in the relative intensities of the SERS bands in comparison to the corresponding Raman ones. In the low wavenumber region of the SERS spectra (see Figure 5 insets), one can observe the presence of the new band around 230 cm^{-1}, which is the clear signature of the molecule–metal interaction. In addition to this band, one can see the out-of-plane deformation of the $C_{38}N_{17}N_{19}$ $N_{18}N_{16}$ ring at 194 cm^{-1} (see Figure 5 inset). This one is highly amplified up to 10^{-4} M, but at lower concentrations, its enhancement vanishes. In contrast, the band at 440 cm^{-1} due to the in-plane deformation of the same ring is visibly more amplified at lower concentrations (10^{-5} and 10^{-6} M) and slightly amplified

from 10^{-2} M to 10^{-4} M. Thus, by analyzing the SERS spectra in comparison to the Raman spectrum, one can affirm that the antibiotic molecule is chemisorbed to the AuNPs.

Table 3. Selected wavenumbers (cm^{-1}) and assignment of the vibrational modes of cefoperazone to the SERS bands at different concentrations.

Raman	SERS on AuNPs		SERS on AgNPs		
	Conc < 10^{-4}	**Conc ≥ 10^{-4}**	**Conc < 10^{-5}**	**Conc ≥ 10^{-5}**	
212		194		190	Out-of-plane deformation of $C_{38}N_{17}N_{19}$ $N_{18}N_{16}$ ring
	228		234		Au/Ag-N vibration
	440 m	440 w		428 w	In-plane deformation of $C_{38}N_{17}N_{19}$ $N_{18}N_{16}$ ring
697 m		706 m		710 w	$C_{38}N_{19}N_{18}$ twist + $N_{17}N_{19}$ N_{18} twist
810 m	803 m		807 m		Wagging of H atoms from the aromatic ring
946 w	913 m		916 m		$N_{18}N_{16}$ str + $C_{38}N_{17}N_{19}$ sym str
1077 w		1080 m		1082 m	$N_{17}N_{19}N_{18}$ asym str
1170 w	1160 s		1170 w	1170 m	Twisting of H atoms from the aromatic ring
1188 w	1183 s				
1283 s	1283 m	1283 s	1284 w	1284 s	$N_{18}N_{19}$ str
1355 m	1364 s	1365 m			$H_{61}C_{39}H_{62}$ wag + $H_{57}C_{33}H_{5}6$ wag + $H_{54}C_{32}H_{55}$ twist
1388 m	1388 s	1392 m		1385 m	$C_{23}N_{11}$ str + $C_{38}N_{17}$ str + $O_5C_{29}H_{58}$ scissoring
1447 w	1425 s	1448 m		1447 m	$C_{37}N_{15}$ str + $H_{56}C_{32}H_{57}$ wag
1486 w	1491 m				Scissoring of H atoms of the benzene ring
	1541 m		1545 s		$C_{26}N_{12}$ str
			1556 s	1556 m	$C_{31}N_{13}$ str
	1593 m		1586 s		Asymmetric stretching of the aromatic ring
1621 s	1619 s		1633 s		Symmetric stretching of the aromatic ring

str = stretching, wag = wagging, twist =twisting, rock = rocking, sym = symmetrical, asym = asymmetrical.

It is evident that there is a notable distinction in the SERS spectra at various concentrations. Beginning from 10^{-5} M, the spectrum undergoes a transformation in its appearance. New bands are amplified, while others experience a decrease in intensity. These changes are associated with different orientations of the adsorbed molecules with respect to the metallic surface according to the SERS selection rules [42–47]. Thus, in line with these rules, if the molecular axis (*z*-axis) is normal to the surface, then vibrations of the adsorbed molecule, which have a polarizability tensor component along this axis, will be preferentially enhanced. Due to its low symmetry, the cefoperazone molecule exhibits polarizability tensor components along the *z*-axis for all vibrations. However, stretching vibrations are supposed to have a larger component along the bond axis, and consequently, stretches that are orthogonal to the surface will result in enhanced intensities in SERS spectra [43], while Raman modes with polarizability tensor components oriented parallel to the surface will exhibit lower intensity [47]. Hence, we can conclude that at lower concentrations, the antibiotic undergoes a reorientation relative to the roughened surface.

It can be seen that in the 10^{-5} M and 10^{-6} M spectra, the most enhanced bands are the ones at 1620 cm^{-1} due to the stretching vibration of the benzene ring, at 1491 cm^{-1} given by the scissoring motion of the H atoms of the aromatic ring, at 1425 and 1388 cm^{-1} assigned to the stretching vibrations of the $C_{37}N_{15}$, $C_{23}N_{11}$ and $C_{38}N_{17}$ bonds, respectively, and around 1170 cm^{-1} attributed to the deformation vibration of the benzene ring H atoms. Moreover, the band at 913 cm^{-1} corresponding to the N_{18}-N_{16} bond stretching mode is also enhanced whereas the intensity of the one at 1283 cm^{-1} corresponding to the N_{18}-N_{19} bond stretching vibration slightly diminished. The shift to lower wavenumber values of the band at 913 cm^{-1} as compared to the corresponding one in the Raman spectrum (at 946 cm^{-1}) can be due to the cefoperazone chemisorption on the metal surface through the nitrogen atoms of the ring, which caused a delocalization of the electrons, and consequently a weakening of the N_{18}-N_{16} and C_{38}-N_{17}-N_{19} bonds' strength. Similar shifts of over 30 cm^{-1} were also observed for bands assigned to ring stretching or in-plane bending vibrations in SERS spectra of other compounds containing the nitrogen ring adsorbed on colloidal

AgNPs [48,49]. Moreover, in the low wavenumber region of the spectra, one can see that the intensity of the band assigned to out-of-plane vibration of the nitrogen ring diminished, while the intensity of the band around 220 cm^{-1} (see Figure 5 inset) increased probably due to a stronger interaction that occurs between the nitrogen atoms of the ring and the AuNPs surface.

The possible orientations of the cefoperazone molecule with respect to the AuNPs surface are depicted in Figure 7. It can be seen that in the first case, at concentrations in the range of 10^{-2}–10^{-4} M, the strongest enhancement is explained by the perpendicular orientation of the N_{18}=N_{19} bond. The enhancement of other stretching but also out-of-plane vibrational modes of the nitrogen ring suggests the tilted orientation of this ring relative to the metal surface. The other vibrational modes are not so strongly enhanced because of the distance between the surface and the rest of the molecule as can be seen from Figure 6. On the other hand, the change in orientation of the adsorbed molecules at 10^{-5} and 10^{-6} M as suggested in Figure 6 would explain the multitude of newly enhanced vibrations, as they lie closer to the surface, as well as the peculiar amplification of the band at 1622 cm^{-1}, corresponding to the symmetric stretching of the benzene ring. At these concentrations, the nitrogen ring adopts a more perpendicular orientation relative to the AuNP surface allowing a stronger interaction between the nitrogen atoms and the metal nanoparticles.

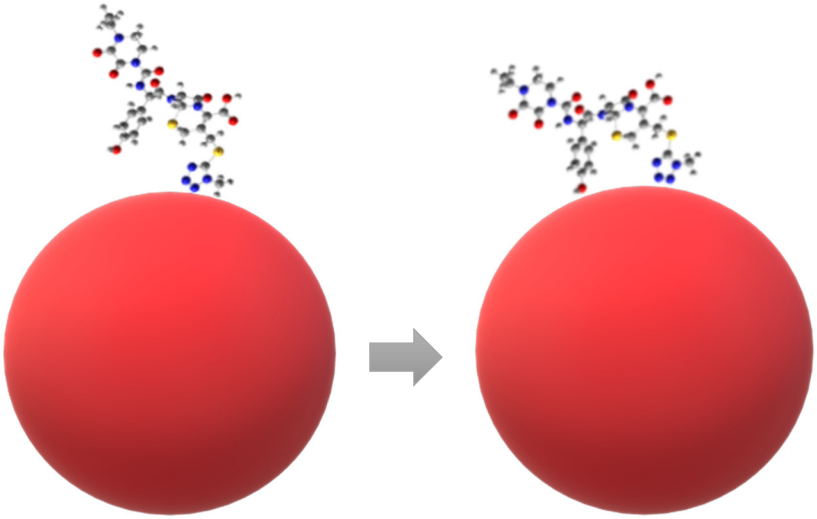

Figure 7. The proposed model of the change in orientation of the cefoperazone molecule with respect to the gold nanoparticles.

The set of spectra depicted in Figure 6 shows the enhancement of vibrational modes given by the cefoperazone adsorbed on the AgNP surface. Just as in the case of the spectra recorded on AuNPs, the band at 1283 cm^{-1}, due to the stretching vibration of the $N_{18}N_{19}$ bond, is strongly enhanced from 10^{-2} M to 10^{-5} M, but lowers in intensity as the concentration decreases to 10^{-6} M. Moreover, one can notice the band at 1080 cm^{-1} assigned to the asymmetric stretching vibration of the $N_{17}N_{19}N_{18}$ group. The band at 697 cm^{-1} in the Raman spectrum is enhanced and shifted to 710 cm^{-1} in the SERS spectra at concentrations higher than 10^{-4} M. It corresponds to the double-twisting of the C_{38}=N_{17}-N_{19} and N_{17}-N_{19}=N_{18} bonds. Moreover, two other bands are slightly shifted and enhanced in these SERS spectra, corresponding to vibrations of the same nitrogen ring. One occurs at 1080 cm^{-1}, assigned to the $N_{17}N_{19}N_{18}$ asymmetric stretching vibration. The other one is at 1385 cm^{-1} and corresponds to the stretching mode of the $C_{38}N_{16}$ band, originally taking place at 1388 cm^{-1}. The double-twisting vibration within the nitrogen ring at 697 cm^{-1} is also found in the SERS spectra of the cefoperazone, shifted in the same way as in the spectra recorded on AuNPs, proving a similar behavior of the molecule with respect to the AgNPs. These shifts and changes in relative intensities of the bands assigned to nitrogen ring vibrations lead us to believe that the adsorption is also taking place through

the nitrogen ring. Looking at the spectra, it seems like the most striking changes appear in the spectrum belonging to the lowest concentrations. The most prominent band is not the one at 1283 cm^{-1} anymore. The strongest amplification belongs now to the newly enhanced bands. The band at 1622 cm^{-1}, corresponding to the symmetric stretching of the benzene ring, is enhanced, and also a few new bands seem to appear throughout the SERS spectra, at 1542 and 1556 cm^{-1}, and 1586 cm^{-1} assigned to the stretching vibration of $C_{26}N_{12}$ and $C_{31}N_{13}$ bonds and asymmetric stretching vibration of the benzene ring.

As in the previous case, most likely the molecule changes its orientation with respect to the AgNP surface as the antibiotic concentration decreases. Thus, at higher concentrations, the molecule adopts a perpendicular orientation of the N_{18}=N_{19} bond relative to the AgNP surface, while the overall nitrogen ring adopts a slightly tilted orientation. With decreasing the concentration to 10^{-6} M, the molecule orientation changes relative to the metal surface so that some other parts of the molecule get closer to the AgNP surface. In this manner, bands that were not even present in the Raman spectrum initially, are enabled to be seen now, as a change in polarizability occurs due to the strong electric fields. Moreover, at this concentration the interaction between the nitrogen atoms and the silver surface is increased as the intensity of the band around 234 cm^{-1} is enhanced (see Figure 6 inset).

As we already mentioned, the theoretical results were in good agreement with the experimental ones, allowing us to assign the vibrational wavenumbers more easily and accurately. This analysis resulted in identifying a fingerprint of the antibiotic, which could be used for its detection in biological fluids or wastewater. Even more, because the SERS spectra are now readily available, cefoperazone could be detected even at concentrations found in the biological fluids.

The SERS spectra exhibit a reduced number of bands for both types of colloids due to the selective enhancement dictated by the selection rules. When concentrations are lower, the shape of the SERS spectra undergoes alterations. The previously enhanced bands display decreased intensity, while new bands emerge that were not initially present in the Raman spectrum of the pristine sample. This observation suggested that the molecule undergoes a change in orientation at concentrations below 10^{-4}–10^{-5} M, leading to these spectral variations.

Initially, the two sulfur atoms in the molecule were of particular interest for the SERS analysis. Sulfur, particularly in thiol groups, is known to have a strong affinity for AuNPs [25,32]. Consequently, we anticipated a similar behavior in the case of cefoperazone, where adsorption on the gold surface would occur via the sulfur atoms. However, the experimental results did not align with these expectations. It is likely that the geometry of the molecule, as depicted in the electronic cloud in Figure 3, creates steric hindrance, rendering the sulfur atoms less accessible to the nanostructured surface.

On the other hand, as mentioned earlier in this paper, the β–lactam ring plays a major role in the destruction of the cellular wall of the bacteria. The carboxylate group was reported to manifest chemisorption to the silver colloid in the case of benzylpenicillin [50]. However, in our case, the molecule chemisorption seems to take place through the nitrogen ring. If the adsorption to the nanoparticle does not interfere with the β–lactam group, it means that the binding of cefoperazone to both the metallic nanoparticle and the bacteria can take place. The implications of this double binding could lead to a boost in the antibacterial effect of cefoperazone, as the whole antibiotic–nanoparticle complex would act against the bacteria.

4. Conclusions

Throughout this study, a comprehensive vibrational analysis of cefoperazone was carried out by means of Raman and FT-IR spectroscopy combined with DFT calculations. Moreover, the adsorption behavior of the antibiotic on the AuNPs and AgNP surface was unraveled. The SERS spectra analysis proved that cefoperazone chemisorption on both types of metal surface occurs through the nitrogen ring and the changes evidenced in the spectra recorded at different concentrations are due to a reorientation of the adsorbed

species relative to the metal surface. No evidence of enhancement related to the β–lactam ring has been observed, indicating that this particular functional group is not involved in the binding of the antibiotic to the nanoparticles. Thus, if the adsorption to the nanoparticle does not interfere with the β–lactam group, the binding of cefoperazone to both the nanoparticle and the bacteria can take place. Considering that the β–lactam ring plays a major role in the destruction of the cellular wall of the bacteria and both AgNPs and AuNPs have an antibacterial effect this double binding of cefoperazone to the metallic nanoparticle and the bacteria could lead to a boost in its antibacterial effect, as the whole antibiotic–nanoparticle complex would act against the bacteria. Therefore, we can conclude that this study represents a point of departure in exploring the potential of both cefoperazone and nanoparticles in the field of biomedicine. It also reasserts the advantages of using SERS as a major tool in research studies of antibiotics.

Supplementary Materials: The following supporting information can be downloaded at: https://www.mdpi.com/article/10.3390/chemosensors12030048/s1, Figure S1: The UV-VIS absorption spectrum of silver (a) and gold (b) colloid; Figure S2: The Raman spectrum of silver and gold colloids; Figure S3: Experimental and theoretical (BPW91 and B3LYP) FT-IR (a) and Raman (b) spectra of cefoperazone in the high wavenumber region.

Author Contributions: Conceptualization, S.A.-M.F. and M.B.; methodology, S.A.-M.F. and M.B.; investigation, S.A.-M.F., Z.-R.T. and K.M.; writing—original draft preparation, S.A.-M.F.; writing—review and editing, Z.-R.T., K.M. and M.B.; visualization, S.A.-M.F.; supervision, M.B. All authors have read and agreed to the published version of the manuscript.

Funding: This research received no external funding.

Institutional Review Board Statement: Not applicable.

Informed Consent Statement: Not applicable.

Data Availability Statement: Data are available upon request.

Conflicts of Interest: The authors declare no conflicts of interest.

References

1. Jones, R.N.; Barry, A.L. Cefoperazone: A Review of Its Antimicrobial Spectrum, fJ-Lactamase Stability, Enzyme Inhibition, and Other in Vitro Characteristics. *Rev. Infect. Dis.* **1983**, *5* (Suppl. S1), S108–S126. [CrossRef]
2. Sader, H.S.; Caravalhes, C.G.; Streit, J.M.; Castanheira, M.; Flamm, R.K. Antimicrobial activity of cefoperazone-sulbactam tested against Gram-Negative organisms from Europe, Asia-Pacific, and Latin America. *Int. J. Infect. Dis.* **2020**, *91*, 32–37. [CrossRef]
3. Lan, S.H.; Chao, C.M.; Chang, S.P.; Lu, L.C.; Lai, C.C. Clinical Efficacy and Safety of Cefoperazone-Sulbactam in Treatment of Intra-Abdominal Infections: A Systematic Review and Meta-Analysis. *Surg. Infect.* **2021**, *22*, 763–770. [CrossRef]
4. Abdullah, F.E.; Mushtaq, A.; Irshad, M.; Rauf, H.; Afzal, N.; Rasheed, A. Current efficacy of antibiotics against Klebsiella isolates from urine samples—A multi-centric experience in Karachi. *Pak. J. Pharm. Sci.* **2013**, *26*, 11–15.
5. Naga, N.G.; El-Badan, D.E.; Rateb, H.S.; Ghanem, K.M.; Shaaban, M.I. Quorum Sensing Inhibiting Activity of Cefoperazone and Its Metallic Derivatives on Pseudomonas aeruginosa. *Front. Cell. Infect. Microbiol.* **2021**, *11*, 716–789. [CrossRef]
6. Gordon, A.J.; Phyfferoen, M. Cefoperazone Sodium in the Treatment of Serious Bacterial Infections in 2100 Adults and Children: Multicentered Trials in Europe, Latin America, and Australasia. *Clin. Infect. Dis.* **1983**, *5* (Suppl. S1), S188–S199. [CrossRef]
7. Giguere, S.; Prescott, J.F.; Dowling, P.M. *Antimicrobial Therapy in Veterinary Medicine*, 5th ed.; Wiley-Blackwell: Hoboken, NJ, USA, 2013; p. 154, ISBN 9780470963029.
8. Rusu, E.A.; Magyari, K.; Baia, L.; Baia, M. Vibrational analysis of α-lipoic acid and its adsorption behavior study by SERS. *J. Mol. Struct.* **2022**, *1248*, 131501. [CrossRef]
9. Chiş, M.; Bonifacio, A.; Sergo, V.; Căinap, C.; Chiş, V.; Baia, M. Experimental and Theoretical Investigations of the Chemotherapeutic Drug Capecitabine. *J. Mol. Struct.* **2022**, *1250*, 131577. [CrossRef]
10. Ivashchenko, O.; Jurga-Stopa, J.; Coy, E.; Peplinska, B.; Pietralik, Z.; Jurga, S. Fourier transform infrared and Raman spectroscopy studies on magnetite/Ag/antibiotic nanocomposites. *Appl. Surf. Sci.* **2016**, *364*, 400–409. [CrossRef]
11. Filgueiras, A.L.; Paschoal, D.; Dos Santos, H.F.; Sant'Ana, A.C. Adsorption study of antibiotics on silver nanoparticle surfaces by surface-enhanced Raman scattering spectroscopy. *Spectrochim. Acta Part A Mol. Biomol. Spectrosc.* **2015**, *136*, 979–985. [CrossRef]
12. Balan, C.; Pop, L.-C.; Baia, M. IR, Raman and SERS analysis of amikacin combined with DFT-based calculations. *Spectrochim. Acta Part A Mol. Biomol. Spectrosc.* **2019**, *214*, 79–85. [CrossRef] [PubMed]

13. Baia, M.; Astilean, S.; Iliescu, T. *Raman and SERS Investigations of Pharmaceuticals*; Springer: Berlin/Heidelberg, Germany, 2008; p. 214, ISBN 978-3-540-78282-7. [CrossRef]
14. Vetrivelan, V.; Sakthivel, S.; Muthu, S.; Al-Saadi, A.A. Non-covalent interaction, adsorption characteristics and solvent effect of procainamide anti-arrhythmias drug on silver and gold loaded silica surfaces: SERS spectroscopy, density functional theory and molecular docking investigations. *RSC Adv.* **2023**, *13*, 9539–9554. [CrossRef]
15. Al-Otaibi, J.S.; Sheena Mary, Y.; Shyma Mary, Y.; Krátký, M.; Vinsova, J.; Gamberini, M.C. DFT, TD-DFT and SERS analysis of a bioactive benzohydrazide's adsorption in silver hydrosols at various concentrations. *J. Mol. Liq.* **2023**, *373*, 121243. [CrossRef]
16. Muniz-Miranda, M.; Muniz-Miranda, F.; Menziani, M.C.; Pedone, A. Can DFT Calculations Provide Useful Information for SERS Applications? *Molecules* **2023**, *28*, 573. [CrossRef]
17. Fornasaro, S.; Cialla-May, D.; Sergo, V.; Bonifacio, A. The Role of Surface Enhanced Raman Scattering for Therapeutic Drug Monitoring of Antimicrobial Agents. *Chemosensors* **2022**, *10*, 128. [CrossRef]
18. Liu, C.; Weber, S.; Peng, R.; Wu, L.; Zhang, W.S.; Luppa, P.B.; Popp, J.; Cialla-May, D. Toward SERS-based therapeutic drug monitoring in clinical settings: Recent developments and trends. *TrAC Trends Anal. Chem.* **2023**, *164*, 117094. [CrossRef]
19. Villa, N.S.; Picarelli, C.; Iacoe, F.; Zanchi, C.G.; Ossi, P.M.; Lucotti, A.; Tommasini, M. Investigating Perampanel Antiepileptic Drug by DFT Calculations and SERS with Custom Spinning Cell. *Molecules* **2023**, *28*, 5968. [CrossRef]
20. Brasil, M.L.; Filgueiras, A.L.; Barros-Pinkelnig, M.; Neves, M.L.; Eugenio, M.; Sena, L.A.; Sant'Anna, C.B.; Silva, V.; Diniz, C.G.; Sant'Ana, A.C. Synergism in the Antibacterial Action of Ternary Mixtures Involving Silver Nanoparticles, Chitosan and Antibiotics. *J. Braz. Chem. Soc.* **2019**, *29*, 2026–2033. [CrossRef]
21. Vo, K.Q.; Tran, M.V.; Nguyen, T.A.; Cao, A.-T.T.; Vu, S.V.; Tran, K.N.; Si, N.T.; Pham, V.-N. Controlled synthesis of spinous gold nanoparticles and their use for surface-enhanced Raman scattering (SERS) detection of the antibiotic sulfathiazole. *New J. Chem.* **2023**, *47*, 6833–6843. [CrossRef]
22. Kha, T.N.; Si, N.T.; Tran, V.M.; Vo, K.Q.; Nguyen, M.T.; Nhat, P.V. Binding Mechanism and Surface-Enhanced Raman Scattering of the Antimicrobial Sulfathiazole on Gold Nanoparticles. *ACS Omega* **2023**, *8*, 43442–43453. [CrossRef]
23. Zhang, M.-A.; Zhou, Z.-M.; Xu, J.; Wang, W.-L.; Pu, S.-H.; Hu, W.-Y.; Luo, P.; Tian, Z.-Q.; Gong, Z.-B.; Liu, G.-K. Qualitative analysis of trace quinolone antibiotics by SERS with fine structure dependent sensitivity. *Spectrochim. Acta Part A Mol. Biomol. Spectrosc.* **2022**, *278*, 121365. [CrossRef] [PubMed]
24. Liu, C.; Müller-Bötticher, L.; Liu, C.; Popp, J.; Fischer, D.; Cialla-May, D. Raman-based detection of ciprofloxacin and its degradation in pharmaceutical formulations. *Talanta* **2022**, *250*, 123719. [CrossRef] [PubMed]
25. Miller, L.M.; Simmons, M.D.; Silver, C.D.; Krauss, T.F.; Thomas, G.H.; Johnson, S.D.; Duhme-Klair, A.-K. Antibiotic-functionalized gold nanoparticles for the detection of active β-lactamases. *Nanoscale Adv.* **2022**, *4*, 573–581. [CrossRef] [PubMed]
26. Ali, H.R.H.; Ali, R.; Batakoushy, H.A.; Derayea, S.M. Solid-State FTIR Spectroscopic Study of Two Binary Mixtures: Cefepime-Metronidazole and Cefoperazone-Sulbactam. *J. Spectrosc.* **2017**, *2017*, 5673214. [CrossRef]
27. Anacona, J.R.; Bravo, A.; Lopez, M.E. Cefoperazone metal complexes: Syn-thesis and characterization. *J. Chil. Chem. Soc.* **2013**, *58*, 1520–1523. [CrossRef]
28. Auda, S.H.; Mrestani, Y.; Fetouh, M.I.; Neubert, R.H.H. Characterization and activity of cephalosporin metal complexes. *Die Pharm.-Int. J. Pharm. Sci.* **2008**, *63*, 555–561.
29. Markina, N.E.; Ustinov, S.N.; Zakharevich, A.M.; Markin, A.V. Copper nanoparticles for SERS-based determination of some cephalosporin antibiotics in spiked human urine. *Anal. Chim. Acta* **2020**, *1138*, 9–17. [CrossRef]
30. Markina, N.E.; Markin, A.V. Application of Aluminum Hydroxide for Improvement of Label-Free SERS Detection of Some Cephalosporin Antibiotics in Urine. *Biosensors* **2019**, *9*, 91. [CrossRef]
31. Han, Y.; Qian, J.; Zhang, J.; Hu, C.; Wang, C. Structure-toxicity relationship of cefoperazone and its impurities to developing zebrafish by transcriptome and Raman analysis. *Toxicol. Appl. Pharmacol.* **2017**, *327*, 39–51. [CrossRef]
32. Lee, P.C.; Meisel, D. Adsorption and surface-enhanced Raman of dyes on silver and gold sols. *J. Phys. Chem.* **1982**, *86*, 3391–3395. [CrossRef]
33. Turkevich, J.; Stevenson, P.C.; Hillier, J. The Formation of Colloidal Gold. *J. Phys. Chem.* **1953**, *57*, 670–673. [CrossRef]
34. Frisch, M.J.; Trucks, G.W.; Schlegel, H.B.; Scuseria, G.E.; Robb, M.A.; Cheeseman, J.R.; Scalmani, G.; Barone, V.; Mennucci, B.; Petersson, G.A.; et al. *"Gaussian 09"*; Gaussian, Inc.: Wallingford, CT, USA, 2009.
35. Dobson, J.F.; Vignale, G.; Das, M.P. (Eds.) *Electronic Density Functional Theory*; Springer: Boston, MA, USA, 1998; p. 81.
36. Piela, L. *Ideas of Quantum Chemistry*, 3rd ed.; Elsevier: Berlin/Heidelberg, Germany, 2020; Volume 2, p. 220.
37. Kim, S.Y.; Joo, T.H.; Suh, S.W.; Kim, M.Y.J. Surface-enhanced Raman scattering (SERS) of nucleic acid components in silver sol: Adenine series. *Raman Spectrosc.* **1986**, *17*, 381. [CrossRef]
38. Chowdhury, J.; Ghosh, M.; Pal, M.; Misra, T.N. Concentration dependent surface enhanced resonance Raman scattering of a porphyrin derivative adsorbed on colloidal silver particles. *J. Colloid Interface Sci.* **2003**, *263*, 318–326. [CrossRef]
39. Moskovits, M.; Suh, J.S. Surface geometry change in 2-naphthoic acid adsorbed on silver. *J. Phys. Chem.* **1988**, *92*, 6327–6329. [CrossRef]
40. Pergolese, B.; Bigotto, A. Surface enhanced Raman spectroscopic studies of 1H- indazole on silver sols. *Spectrochim. Acta* **2001**, *57*, 1191–1197. [CrossRef]
41. Sheena Mary, Y.; Shyma Mary, Y.; Krátký, M.; Vinsova, J.; Baraldi, C.; Gamberini, M.C. DFT, SERS-concentration and solvent dependent and docking studies of a bioactive benzenesulfonamide derivative. *J. Mol. Struct.* **2021**, *1228*, 129680. [CrossRef]

42. Moskovits, M.; DiLella, D.P. Surface-enhanced Raman spectroscopy of benzene and benzene-d6 adsorbed on silver. *J. Chem. Phys.* **1980**, *73*, 6068–6075. [CrossRef]
43. Gao, P.; Weaver, M.J. Surface-enhanced Raman spectroscopy as a probe of adsorbate surface bonding: Benzene and monosubstituted benzenes adsorbed at gold electrodes. *J. Phys. Chem.* **1985**, *89*, 5040–5046. [CrossRef]
44. Creighton, J.A. Surface raman electromagnetic enhancement factors for molecules at the surface of small isolated metal spheres: The determination of adsorbate orientation from SERS relative intensities. *Surf. Sci.* **1983**, *124*, 209–219. [CrossRef]
45. Chulhai, D.V.; Jensen, L. Determining Molecular Orientation with Surface-Enhanced Raman Scattering Using Inhomogenous Electric Fields. *J. Phys. Chem. C* **2013**, *117*, 19622–19631. [CrossRef]
46. Moskovits, M. Surface selection rules. *J. Chem. Phys.* **1982**, *77*, 4408–4416. [CrossRef]
47. Cialla, D.; März, A.; Böhme, R.; Theil, F.; Weber, K.; Schmitt, M.; Popp, J. Surface-enhanced Raman spectroscopy (SERS): Progress and trends. *Anal. Bioanal. Chem.* **2012**, *403*, 27–54. [CrossRef]
48. Thomas, S.; Biswas, N.; Venkateswaran, S.; Kapoor, S.; Naumov, S.; Mukherjee, T. Studies on Adsorption of 5-Amino Tetrazole on Silver Nanoparticles by SERS and DFT Calculations. *J. Phys. Chem. A* **2005**, *109*, 9928–9934. [CrossRef] [PubMed]
49. Saegmueller, B.; Freunscht, P.; Schneider, S. The assignment of the vibrations of substituted mercaptotetrazoles based on quantum chemical calculations. *J. Mol. Struct.* **1999**, *482–483*, 231–235. [CrossRef]
50. Iliescu, T.; Baia, M.; Pavel, I. Raman and SERS investigations of potassium benzylpenicillin. *J. Raman Spectrosc.* **2006**, *37*, 318–325. [CrossRef]